Design of a Fluidic Circuit-Based Microcytometer for Circulating Tumor Cell Detection and Enumeration

Jinhong Guo, Wen Lei, Xing Ma, Peng Xue, Yu Chen, and Yuejun Kang

***Abstract*—Portable devices have been introduced to provide companion diagnostics in many applications such as personalized healthcare monitoring since several decades ago. Recently the polydimethylsiloxane (PDMS)-based microfluidic chip enables a cost effective platform for point of care diagnostics. In this paper, we present a systematic theoretical and experimental study of a novel fluidic circuit-based microcytometer. The working principle of this device is based on the characterization of the bandwidth and amplitude of the bias-voltage pulses induced by the microparticle's physical blockage of the sensing aperture. In the simulation, the amplitude and bandwidth of the bias voltage change is simply related to the microparticle translocation time and resistance change in the sensing aperture. In the modeling part, we simulate the two parameters (peak and translocation time) by considering 7 μm and 16 μm, which is used to approximately characterize the Red Blood Cells (RBCs) and Circulating Tumor Cells (CTCs). In the experimental setup, microparticles of different sizes are used to demonstrate the chip performance. Furthermore, RBCs and CTCs are detected and enumerated by the proposed chip. The microcytometry chip is presented and is expected toward the point of care clinical diagnostics.**

***Index Terms*—Circulating tumor cell, microcytometer, personalized healthcare, point of care, polydimethylsiloxane (PDMS) chip.**

I. Introduction

IT has been well known that circulating tumor cells (CTCs) play a critical role in the cancer metastasis, in which the CTCs are shed from the primary tumor and transported through blood circulation until they invade the distant organs [1]–[3]. These cells have been detected in the blood samples of many cancer patients with metastatic disease, however with extremely low concentration on the order of 1–10 per ml of whole blood. Since the number of metastases formed is generally proportional to number of CTCs shed into circulation, accurate CTC counting in the blood samples can provide a noninvasive measure to monitor the disease progression and treatment efficacy.

Flow cytometry has become the gold standard for clinical hematologic assay after development of half a century. Conventional flow cytometry requires the specific fluorescent dyes to stain the target cells for counting and detection [4], [5]. By comparing three optical signals, namely forward scatter (FSC), side scatter (SSC), and fluorescence signal (FL), statistical information of cells type, size, and population, can be obtained in a few minutes. Although the flow cytometry is a highly powerful technology, the cost however is intimidating. As a typical and popular flow cytometer, a Beckman-Coulter FC500 has a price tag of US$100,000. In addition, the fluorescent labeling procedure makes the sample preprocessing highly labor-intensive and time consuming, therefore significantly limiting its capability for point of care diagnosis. On the other hand, the resistive pulse sensor based on Coulter principle has emerged as a cost effective platform for biological particles counting and detection in a completely fluidic environment [6]–[8]. This technique has been widely for the investigations of pollen [9], biological cells [10], bacteria [11], viruses [12], DNA and other biomolecules [13]–[15]. The working principle is based on the fact that, when a particle carried by the fluid translocates a micro/nano scale aperture, the electrical impedance of the aperture will significantly increase due to the blockage by the particle, resulting in the significant change of the electrical current (a pulse) across the aperture. Every single pulse corresponds to an event of a single particle; while the higher pulse amplitude implies larger particle size. By characterizing the amplitude and the bandwidth of the electrical pulses, statistical information of the size and the numbers of the microparticles can be obtained. Recently, with the advance of micro/nanofabrication technology, solid-state micropores have been demonstrated with excellent capability for analysis of whole blood cells and cancer cells [6]. The microfluidic impedance cytometry enables a highly cost-effective solution for point of care characterization of CTCs [16]. It is expected that the next generation of impedance microcytometry will be equipped with multiple microfluidic channels that can achieve much higher throughput for screening tumor cells in whole blood sample.

In this paper, based on the same Coulter principle, a bias-voltmeter was used for microparticles counting and enumeration.

Manuscript received April 30, 2013; revised July 04, 2013; accepted July 14, 2013. This research was supported by a research grant from Nanyang Technological University College of Engineering and Academic Research Fund from Ministry of Education of Singapore (RG 26/11) awarded to Y. Kang, and A*STAR research grant [2nd JCO career Development Award (CDA) Grant Call 12302] awarded to J. Guo. Y. Chen acknowledges the Ph.D. scholarship from Nanyang Technological University. The authors declare no financial or commercial conflicts of interest. This paper was recommended by Associate Editor S. T. C. Wong.

J. Guo is with the Institute of Microelectronics, A*STAR, Singapore 117685, and also with the School of Chemical and Biomedical Engineering, Nanyang Technological University, Singapore 637459 (e-mail: jguo002@e.ntu.edu.sg).

W. Lei is with the Department of Electrical and Computer Engineering, National University of Singapore, Singapore 117576 (e-mail: leiwen610@gmail.com).

X. Ma is with the School of Materials Science and Engineering, Nanyang Technological University, Singapore 639798 (e-mail: xma4@e.ntu.edu.sg).

P. Xue and Y. Kang are with the School of Chemical and Biomedical Engineering, Nanyang Technological University, Singapore 637459 (e-mail: pxue1@e.ntu.edu.sg; yuejun.kang@ntu.edu.sg).

Y. Chen is with the Institute of Microelectronics, A*STAR, Singapore 117685 (e-mail: cheny1@ime.a-star.edu.sg).

Color versions of one or more of the figures in this paper are available online at http://ieeexplore.ieee.org.

Digital Object Identifier 10.1109/TBCAS.2013.2275091

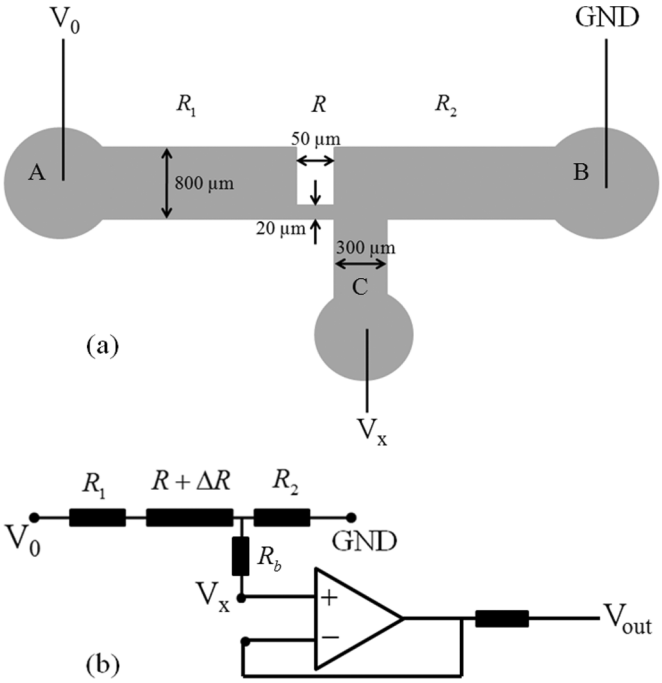

Fig. 1. (a) Design of the microfluidic channel. (b) The equivalent electric circuit of the microfluidic channel.

The carrying fluid was driven by a syringe pump and two electrodes were inserted in the microchannel to provide the electrical bias across the sensing aperture. When a microparticle blocks the sensing aperture temporarily during translocation, the electrical impedance of the aperture changes significantly, resulting in a modulation of the electric bias on the fluidic branch. By characterizing the dynamic modulation of the bias pulse, the particle size and translocation time can be analyzed. A statistical analysis on the data for large population of biological cells can categorize all the cells into different phenotypes.

II. Theory and Method

The structure of the fluidic circuit-based microcytometer in this paper is composed of three reservoirs. As Fig. 1(a) shows, two electrodes are inserted into both ends of a main fluidic channel, respectively. The side branch channel acts as a conducting electrode. The left section of the main channel is 800 μm in width and 6 mm in length; the right section of the main channel is 800 μm in width and 4.7 mm in length. The branch channel has width of 300 μm. The length and width of the sensing aperture are 50 μm and 20 μm, respectively. The entire channel has the same height of 20 μm. The equivalent electric circuit is shown in Fig. 1(b). In the following part, the theoretical analysis and numerical modeling of the pulse amplitude and translocation time are demonstrated.

A. Theoretical Analysis

Since the particle size is much smaller than the channel size in R1 and R2 regimes, the electrical impedance modulation of the particle on these two channel sections are negligible. However, when the particle translocates through the narrow sensing aperture R, it will induce a significant modulation on the aperture impedance because its comparable size causes partial blockage of the aperture. We assume ΔR is the resistance change due to the temporary existence of the microparticle in the aperture. The electric current through the aperture without and with a particle inside can be written as

$$I = \frac{V_0}{R_1 + R_2 + R}; \quad I^* = \frac{V_0}{R_1 + R_2 + R + \Delta R} \tag{1}$$

where V_0 is the total bias across the main channel. The corresponding electrical voltages at the side branch are

$$V_x = IR_2; \quad V_x^* = I^* R_2. \tag{2}$$

The relative change of branch voltage before and after the particle moves in can be derived from (1)–(2)

$$\frac{\Delta V_x}{V_x} = \frac{V_x - V_x^*}{V_x} = \frac{\Delta R}{R_1 + R_2 + R + \Delta R}. \tag{3}$$

Because $\Delta R \ll R_1 + R_2 + R$, the relation between the side branch voltage modulation and the resistance modulation in (3) can be simplified as

$$\Delta V_x = \frac{V_x}{R_1 + R_2 + R} \Delta R. \tag{4}$$

The resistance modulation induced by a spherical particle inside a channel also be related to the particle size as derived by Deblois and Bean [21]

$$\Delta R \approx \frac{24\rho}{\pi^2 D^4} V_p \tag{5}$$

where V_p is the particle volume; ρ is the fluid resistivity; and D is the channel diameter. From the (4)–(5), the amplitude of the voltage modulation is linearly proportional to the particle volume.

B. Numerical Modeling

A 3-D model is developed by using Finite Element Method based commercial software COMSOL Multiphysics®4.3 (COMSOL, CA, USA). In the simulation, the particle is released at upstream location before it transports into the small aperture. The carrying liquid flow is pressure-driven, which leads to a hydrodynamic force on the particle. The particle was also subject to both electrophoretic and dielectrophoretic forces under the applied electrical potential across the channel.

1) Electrical Field: In the computational domain in Fig. 1(a), since the liquid is neutral electrolyte solution, the electrical field is governed by [17]

$$-\nabla \cdot (\varepsilon_0 \varepsilon_r \nabla \varphi) = 0 \tag{6}$$

where ε_0 is the permittivity of vacuum and ε_r is the relative permittivity of the fluid, respectively; φ is the electrical potential.

The boundary conditions for (6) are given as electrical potentials at the inlet and the outlet

$$\varphi_{in} = 10\ \mathrm{V}; \varphi_{out} = 0\ \mathrm{V}. \tag{7a}$$

The particle surface and the channel wall are assumed non-conducting and rigid, therefore

$$\vec{n} \cdot \nabla\varphi = 0 \tag{7b}$$

where $\vec{n}$ is the normal vector on the particle surface or channel wall. Due to the extremely high input impedance of the measurement equipment (on the order of $\mathrm{G}\Omega$), the resistance of the branch channel (on the order of $\mathrm{M}\Omega$) can be neglected. Therefore, the voltage measured by the sensing electrode can be approximately evaluated by the average voltage at the intersection between the branch and the main channel

$$\overline{V_x} = \frac{\int_S \varphi dS}{S} \tag{8}$$

where S is the area of the intersection.

2) Flow Field: The flow field in the microchannel satisfied the Navier–Stokes equation

$$\rho\left[\frac{\partial\vec{u}}{\partial t} + \vec{u}\cdot\nabla\vec{u}\right] = -\nabla p + \mu\nabla^2\vec{u} \tag{9}$$

and the continuity equation

$$\nabla \cdot \vec{u} = 0. \tag{10}$$

The boundary condition at the channel wall is given by Smoluchowski formula under the assumption that the electrical double layer (EDL) is very thin (nanoscale) compared to the channel size (microscale) [18], [19]

$$\vec{u} = -\frac{\varepsilon_0\varepsilon_r\zeta_w}{\mu}\vec{E}, \quad \vec{n}\cdot\nabla p = 0. \tag{11a}$$

The boundary condition at the particle surface is given by the summation of the particle velocity and the electroosmotic flow velocity [19]

$$\vec{u} = \vec{V_p} - \frac{\varepsilon_0\varepsilon_r\zeta_p}{\mu}\vec{E}, \quad \vec{n}\cdot\nabla p = 0 \tag{11b}$$

$$\text{Channel inlet}: \ \vec{n}\cdot\nabla\vec{u} = 0, v_{inlet} = v_0 \tag{11c}$$

$$\text{Channel outlet}: \ \vec{n}\cdot\nabla\vec{u} = 0, p = 0 \tag{11d}$$

where $\vec{u}$ is flow field; v_0 denotes the inlet flow velocity; ρ is the fluid density; μ is the dynamic viscosity; ζ_{p} and ζ_{w} are the zeta potentials at particle surface and at the channel wall, respectively; $\vec{E}$ is the electrical field and $\vec{V_p}$ is translational velocity of the particle.

3) Particle Motion: When an external potential is applied across the channel, the particle starts to migrate under the hydrodynamic motion and electrophoretic motion. The particle is also subject to dielectrophoretic forces due to the non-uniform electrical field in the sensing aperture. The governing equation of particle motion is given by Newton's second law

$$m_p\frac{d\overrightarrow{V_p}}{dt} = \overrightarrow{F}_{net} \tag{12}$$

where m_{p} is the mass of the particle; $\overrightarrow{F}_{net}$ is the net force acting on the particle. The net force is composed of three main forces: electrophoretic force $\overrightarrow{F}_{EP}$ due to net charge on the particle surface, dielectrophoretic force $\overrightarrow{F}_{DEP}$due to the non-uniform distribution of electrical field near/in the aperture, and the hydrodynamic force $\overrightarrow{F}_h$ due to the flow drag. Consequently, the total net force is described by

$$\overrightarrow{F}_{net} = \overrightarrow{F}_{EP} + \overrightarrow{F}_{DEP} + \overrightarrow{F}_h. \tag{13}$$

The Dielectrophoretic force is expressed by [20]

$$\overrightarrow{F}_{DEP} = -2\pi\varepsilon_f a^3(\overrightarrow{E}\cdot\nabla)\overrightarrow{E} \tag{14}$$

where ε_f is the permittivity of the fluid, a is the particle radius. Theoretically, the flow field can be separated into an inner region and an outer region. Under the assumption of thin EDL as described by Debye length [19], the electroosmotic flow exists close to the particle surface where the local net charge is non-zero. In the outer region, the positive ions are neutralized by the negative ions that results in the local zero charge density. Based upon this assumption, the hydrodynamic force $\overrightarrow{F}_h$ includes contributions from flows in both regions

$$\overrightarrow{F}_h = \overrightarrow{F}_{ho} + \overrightarrow{F}_{hin}. \tag{15}$$

$\overrightarrow{F}_{hin}$ is resulted from the electroosmotic flow in inner region (EDL), while $\overrightarrow{F}_{ho}$ is due to the flow field in outer region. $\overrightarrow{F}_{hin}$ and the electrophoretic force $\overrightarrow{F}_{EP}$ can both be expressed by the same Smoluchowski equation [18], however they have the opposite directions, which implies that these two forces are counterbalanced [19]. Finally, the net force acting on the particle is simplified as

$$\overrightarrow{F}_{net} = \overrightarrow{F}_{DEP} + \overrightarrow{F}_{ho} \tag{16}$$

where the hydrodynamic force in the outer region is calculated by integrating the fluidic stress tensor over the particle surface [11], [19]

$$\overrightarrow{F}_{ho} = -\oiint_S \overline{\overline{\sigma}}_p \cdot \overrightarrow{n} dS \tag{17a}$$

where S is the particle surface, $\bar{\bar{\sigma}}_p$ is the stress tensor described as follows [19]

$$\bar{\bar{\sigma}}_p = -p\bar{\bar{I}} + \mu[\nabla\vec{u} + (\nabla\vec{u})^T]. \tag{17b}$$

The initial condition of particle motion is set to zero.

$$\overrightarrow{V_p}|_{t=0} = 0, \quad \vec{u}|_{t=0} = 0. \tag{17c}$$

In order to simulate the pulse amplitude and translocation time, all the governing equations need to be coupled together during computation. We defined the Poisson equation in COMSOL AC/DC module to solve the electrical field distribution, followed by defining the Navier–Stokes equation in COMSOL CFD module to solve the flow velocity field. These two governing equations are coupled through the electric field strength at the microchannel wall or the particle surface, which determines the boundary flow slip velocity by Smoluchowski equation (11a)—(b). The COMSOL modules can compute instantaneous flow field and electrical field. These parameters are imported into MATLAB (Mathworks, MA, USA) through an interface with COMSOL to compute the net force acting on the particle, followed by calculating the displacement of the particle by the next time loop. The displacement and velocity of the particle are stored by MATLAB and updated to COMSOL through the same interface. Hence, COMSOL can regenerate the updated model and compute the new flow field and electrical field. The computation loop is coded in MATLAB to manage the whole progress until the particle goes beyond a pre-defined distance at the downstream of the sensing aperture. The length of the time loop is adaptive to the particle transient velocity magnitude ($\Delta t \propto 1/|\vec{u}|$). The initial time step is set as 0.5×10^{-6}s. Different mesh sizes were used for different parts of the computation domain. Regular fine mesh grids were constructed for large channels; while extremely fine mesh grids were used for the small sensing aperture area to take into account of the dramatic change of the electric field and the flow field. In the overall computation domain, the maximum mesh size is 10 μm, and the minimum mesh size is 2 μm. The model was run on a computer with 32 GB RAM and Intel Core i-7 Quad processor 3.9 GHz. The major parameters in the numerical simulation are listed in Table I.

TABLE I
MAJOR CONSTANTS USED IN THE NUMERICAL SIMULATION. (FLUID PROPERTIES IS BASED ON 1X PBS SOLUTION AT 20°C)

Relative permittivity of fluid ε_r	80
Permittivity of vacuum ε_0 (C/Vm)	8.854×10^{-12}
Viscosity of fluid μ (kg/ms)	0.9×10^{-3}
Density of fluid ρ (kg/m^3)	998
Zeta potential on particle surface ξ_p (mV) [18]	-40
Zeta potential on channel wall ξ_w (mV) [19]	-50
Aperture width D (μm)	20
Aperture length L (μm)	50
Left channel length L_1 (mm)	6
Right channel length L_2 (mm)	4.7
Channel height H (μm)	20
Particle diameter d (μm)	7, 16

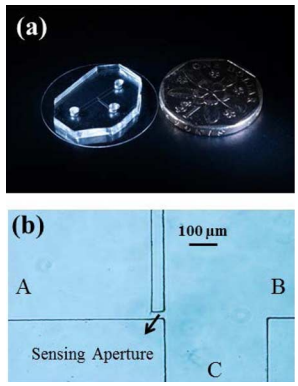

Fig. 2. (a) An actual chip with a dollar coin. (b) A microscopic image of the central structure: a sensing aperture that is 20 μm in width and 50 μm in length.

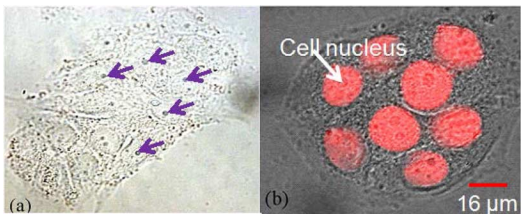

Fig. 3. (a) An image of MCF-7 cells under a light microscope. (b) A fluorescent microscopic image of MCF-7 with red staining.

C. Method

1) Device Fabrication: The microfluidic chip was fabricated by soft lithography. Negative photoresist SU-8 25 (Microchem, MA, USA) was spin-coated on a glass slide and subsequently soft baked (65°C for 5 minutes, 95°C for 15 minutes). After UV light exposure for 20 seconds and post-baking (65°C for 1 minute, 95°C for 5 minutes), the SU-8 master was developed on the glass slides with the thickness of 20 μm. The PDMS (Sylgard 184, Dow Corning, MI, USA) and curing agent with a volume ratio of 10:1 were then mixed well and cast onto the SU-8 mold. After degassing in a vacuum box, the PDMS was moved into an oven and cured at 75°C for 2 hours. Finally, the PDMS replica was peeled off from the mold and bonded with a clean cover slide by plasma treating for 10 seconds. Fig. 2 shows an actual chip and its central structure.

2) Cell Preparation: MCF-7 (American Type Culture Collection, MD, USA) that is derived from breast adenocarcinoma were cultured in Minimum Essential Media (MEM) (Gibco, cat# 11095-080) supplemented with 10% fetal bovine serum (FBS) (Gibco, cat# 10270106), 1 mM sodium pyruvate (Gibco, cat# 11360-070), 0.1 mM MEM non-essential amino acids (Gibco, cat# 11140-050) and grown at 37°C under a 5% CO_2 in a T75 flask (Fig. 3). Low concentration of MCF-7 cells spiked and dispersed in PBS was stored for use. The whole blood was centrifuged under 2000 g for 15 min. The RBCs were obtained at the bottom of the centrifuge tube.

3) Measurement Setup: Fig. 4 shows the typical measurement setup. The fabricated chip was placed under a fluorescent microscope. The device has three reservoirs made for the fluidic interface. The samples were injected from inlet reservoir and the

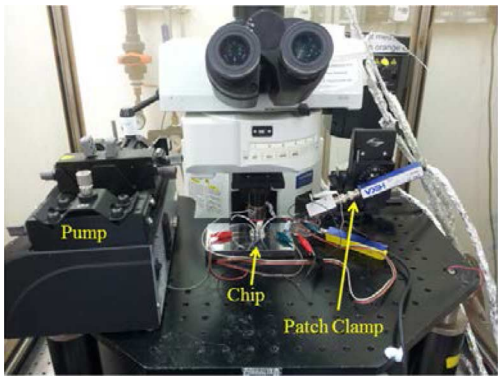

Fig. 4. The system setup for the experiment.

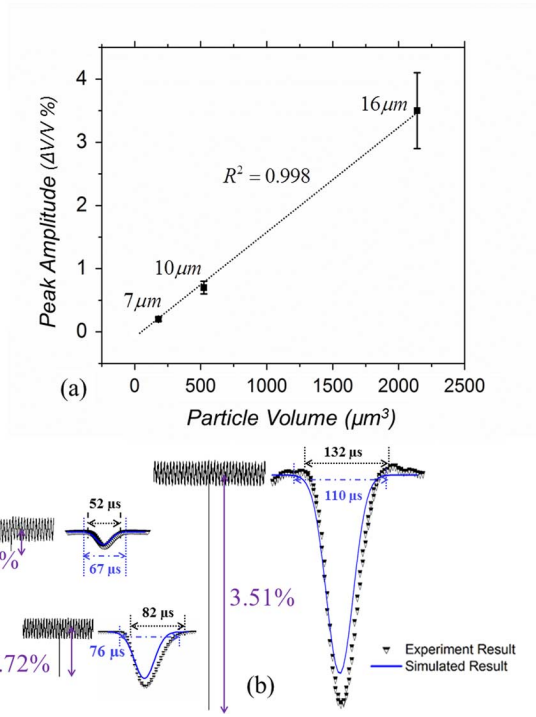

Fig. 5. (a) The peak amplitude changes linearly with the particle volume. The dotted line is a linear regression of the experimental data. (b) Measured and simulated profiles of some individual pulses induced by 7 μm, 10 μm and 16 μm particles. The peak amplitude is evaluated as a percentage modulation based on the baseline voltage at the branch channel.

waste was removed from the outlet reservoir. Three platinum wires were inserted into three reservoirs, respectively. Once the PBS solution primed all the channels, the side branch reservoir was sealed. A syringe pump was used to perfuse the sample flow through the main channel. The electrical bias of the side branch channel was measured under a total bias of 10 V across the main channel by using a patch clamp amplifier (EPC10 USB Quadro, HEKA Electronik, Lambrecht, Germany), which provided accurate detection of the tiny voltage modulation with high signal-to-noise ratio. The data were collected at a sampling rate of 1 MHz and imported into a homemade MATLAB program for post-processing.

III. Results and Discussion

A. Peak Amplitude

As discussed in the theoretical analysis, the change of the branch voltage is linearly proportional to the particle size (volume). Polystyrene particles of various sizes (7 μm, 10 μm and 16 μm) were used to induce the electric voltage modulation of the side branch, and the modulation pulses were recorded and analyzed by the patch clamp system. A good linearity with regression of $\mathrm{R}^2 = 0.998$ was achieved by comparing the measured relative peak amplitude of the voltage pulses to the volume of the particles [Fig. 5(a)]. These results confirmed the prediction in the theoretical analysis (4)–(5), which showed the voltage modulation amplitude is proportional to the particle volume. In other words, this detection mechanism is quite sensitive to the change of particle size, since the electric response increases in the third order of the particle diameter.

B. Peak Amplitude & Translocation Time

The modulation of the electrical resistance in a microchannel caused by the particle blockage has been investigated earlier by many researchers [21], [22]. However, very limited research has been done for systematic simulation and characterization of both the peak amplitude and translocation time. These two parameters are of critical importance in designing the impedance microcytometry. In this section, we present the simulation results for the change of peak amplitude and translocation time due to the translocation of microparticles, and compare them with experimental data. During simulation, we use 7 μm and 16 μm microparticles to approximate the RBCs and CTCs, respectively. However, for simplicity, we did not consider the effects due to deformation of the biological cells. In this simulation, we focus on both the pulse peak amplitude that corresponds to the change of sensing voltage, and the pulse bandwidth that corresponds to the total translocation time through the sensing aperture. Under the condition that very low external voltage (10 V in simulation and experiment) is applied cross the microfluidic channel, the translocation time of the particle is mainly determined by the flow rate of the carrying liquid. The contribution of the electrokinetic flow is much smaller, in terms of magnitude, than the pressure-driven flow. Therefore we can use the hydrodynamic fore for a rough estimation of the translocation time by microparticles of different sizes. The hydrodynamic force is proportional to the surface area of a particle, $F_h \propto r^2$; the particle mass is proportional to the volume, $m \propto r^3$; thus the particle acceleration (F_h/m) is proportional to the scale of r^{-1}, which predicts that a smaller particle accelerates faster than a larger particle during the accelerating motion through the sensing aperture. More accurate predictions by the numerical simulation were summarized in Table II and compared with experimental data.

It can be shown that the simulated translocation time agrees with the above rough analysis, which predicts that a 7 μm particle trends to have shorter translocation time than a 16 μm particle. The same trend was further verified by the experiment data in Table II. Furthermore, the simulation result can provide a method to predict the distribution of cell groups of different

TABLE II
SUMMARY OF THE SIMULATION RESULTS AND THE EXPERIMENTAL DATA FOR DIFFERENT SAMPLE TESTS

	Simulation		Experimental Result (Average)	
Sample types	Peak Amplitude(%)	Translocation Time(μs)	Peak Amplitude(%)	Translocation Time (μs)
Polystyrene particle (7 μm)	0.182	67	0.21±0.03	52±10
RBC	——	——	0.27±0.25	40±21
Polystyrene particle (16 μm)	3.27	110	3.51±0.5	132±30
MCF-7 Tumor Cell	——	——	3.93±1.97	150±51

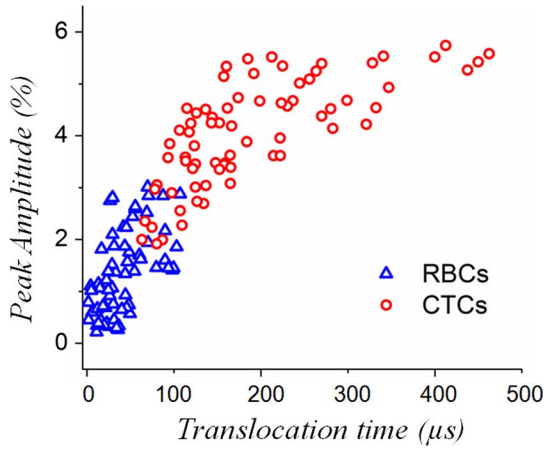

Fig. 6. The distribution of the peak amplitude and translocation time for two types of cells independently through the sensing aperture: RBCs and CTCs.

phenotypes using a spectroscope analysis on the correlation between the peak amplitude and the translocation time, as will be discussed in the next section.

C. Cells Detection and Enumeration

In order to investigate the accuracy of the device, the correlation spectroscope by two parameters, peak amplitude and the translocation time, were analyzed for determination of different cell types. The sample contained RBCs of 1400 cells/ml and CTCs of 2000 cells/ml spiked in 1X PBS solution. The applied DC bias on the chip was 10 V. Totally about 200 cell events, including RBCs and CTCs, were measured and analyzed (Fig. 6). As discussed earlier, the RBCs induce smaller peak amplitude than the CTCs, because CTCs' larger size lead to a greater blockage of the sensing aperture. Fig. 6 shows obvious contrast between these two distinct groups of cells in terms of the correlation between peak amplitude and translocation time. In addition, the translocation time of a single cell, by analyzing the pulse bandwidth, could be another important parameter in characterizing the biological cells using Coulter principle, because it can be related to the cellular physiological characteristics. For instance, if a cell deforms when it squeezes through a small aperture due to the geometrical constriction or the flow shear stress, it becomes longer in shape in the direction of the flow (spheroidal shape), which will effectively increase the translocation time. There is recent evidence indicating that the tumor cells have much higher flexibility and tend to deform more easily compared to other cell types, which could facilitate the tumor cells to penetrate the endothelial barriers and cause metastasis [23], [24] Hence, the translocation time could provide a measure of the cell deformability that may help further differentiate the CTCs from other blood cells of like sizes. Although the cell deformation and its effects on the pulse profile are beyond the scope of this study, the authors may consider this important aspect in a follow-up investigation. This proof-of-concept study shows that the proposed device is capable of providing important information that can help differentiate CTCs from the RBCs, which might contribute to the final goal of detecting extremely rare CTCs from the highly complex background of the whole blood.

IV. CONCLUSION

In this paper, we present the systematic design of the fluidic circuit-based microcytometry for circulating tumor cells detection and enumeration toward the point of care diagnosis, which can concurrently characterize both peak amplitude and translocation time. By correlated analysis of these two parameters, cells with different size can be classified. It's demonstrated that RBCs and CTCs can be detected and classified by the proposed device. We also introduce the numerical model to provide the critical guidance for the development of such microcytometry. In summary, this device and design theory can provides critical insight and guidance for developing the cost effective platform for rapid point of care detection and enumeration of rare cells. Future research effort to further enhance this enabling platform can apply the CMOS technology for integration of micro-electrode arrays in order to interface multiple microfluidic channels on the same chip, which could realize multiplexed biomedical analyses in parallel and significantly improve the overall throughput of the device.

REFERENCES

[1] V. Zieglschmid, C. Hollmann, and O. Bocher, "Detection of disseminated tumor cells in peripheral blood," *Crit. Rev. Clin. Lab. Sci.*, vol. 42, no. 2, pp. 155–196, 2005.

[2] X. Wang, X. Qian, J. J. Beitler, Z. G. Chen, F. R. Khuri, M. M. Lewis, H. J. C. Shin, S. Nie, and D. M. Shin, "Detection of circulating tumor cells in human peripheral blood using surface-enhanced Raman scattering nanoparticles," *Cancer Res.*, vol. 71, no. 5, pp. 1526–1532, Mar. 2011.

[3] E. C. Kohn and L. A. Liotta, "Molecular insights into cancer invasion: Strategies for prevention and intervention," *Cancer Res.*, vol. 55, no. 9, pp. 1856–1862, May 1995.

[4] E. Racila, D. Euhus, A. J. Weiss, C. Rao, J. McConnell, L. Terstappen, and J. W. Uhr, "Detection and characterization of carcinoma cells in the blood," *Natl. Acad. Sci. USA*, vol. 95, no. 8, pp. 4589–4594, Apr. 1998.

[5] N. Watkins, B. M. Venkatesan, M. Toner, W. Rodriguez, and R. Bashir, "A robust electrical microcytometer with 3-dimensional hydrofocusing," *Lab Chip*, vol. 9, no. 22, pp. 3177–3184, 2009.
[6] W. Asghar, Y. Wan, A. Ilyas, R. Bachoo, Y. T. Kim, and S. M. Iqbal, "Electrical fingerprinting, 3D profiling and detection of tumor cells with solid-state micropores," *Lab Chip*, vol. 12, no. 13, pp. 2345–2352, 2012.
[7] M. Sridhar, D. Xu, Y. Kang, A. B. Hmelo, L. C. Feldman, D. Q. Li, and D. Y. Li, "Experimental characterization of a metal-oxide-semiconductor field-effect transistor-based coulter counter," *J. Appl. Phys.*, vol. 103, no. 10, p. 104701, 2008.
[8] Y. N. Wang, Y. Kang, D. Xu, C. H. Chon, L. Barnett, S. A. Kalams, and D. Li, "On-chip counting the number and the percentage of CD4+ T lymphocytes," *Lab Chip*, vol. 8, no. 2, pp. 309–315, 2008.
[9] A. V. Jagtiani, J. Zhe, J. Hu, and J. Carletta, "Detection and counting of micro-scale particles and pollen using a multi-aperture coulter counter," *Meas. Sci. Technol.*, vol. 17, no. 7, pp. 1706–1714, 2006.
[10] S. Zheng, M. Liu, and Y. C. Tai, "Micro coulter counters with platinum black electroplated electrodes for human blood cell sensing," *Biomed. Microdev.*, vol. 10, no. 2, pp. 221–231, 2008.
[11] Y. Wu, D. B. James, and A. Mahmoud, "Micromachined coulter counter for dynamic impedance study of time sensitive cells," *Biomed. Microdev.*, vol. 14, no. 4, pp. 739–750, 2012.
[12] I. Z. Jeffrey, "Impedance-based flow cytometry for the measurement of microparticles," *Semin. Thromb. Hemost.*, vol. 36, no. 8, pp. 819–823, 2010.
[13] J. S. Lorenz, O. Oliver, C. Catalin, G. Joanne, and F. K. Ulrich, "Detecting DNA folding with nanocapillaries," *Nano Lett.*, vol. 10, no. 7, pp. 2493–2497, 2010.
[14] H. Bayley and C. R. Martin, "Resistive-pulse sensing—From microbes to molecules," *Chem. Rev.*, vol. 100, no. 7, pp. 2575–2594, 2000.
[15] C. Dekker, "Solid-state nanopores," *Nat. Nanotechnol.*, vol. 2, no. 4, pp. 209–215, 2007.
[16] H. Choi, K. B. Kim, C. S. Jeon, I. Hwang, S. Lee, H. K. Kim, H. C. Kim, and T. D. Chung, "A label-free DC impedance-based microcytometer for circulating rare cancer cell counting," *Lab Chip*, vol. 13, no. 5, pp. 970–977, 2013.
[17] Y. Kang and D. Li, "Electrokinetic motion of particles and cells in microchannels," *Microfluid Nanofluid*, vol. 6, no. 4, pp. 431–460, 2009.
[18] J. Guo, T. S. Pui, A. R. R. Rahman, and Y. Kang, "3D numerical simulation of a coulter counter array with analysis of electrokinetic forces," *Electrophor.*, vol. 34, no. 3, pp. 417–424, 2013.
[19] Z. Wu, Y. Gao, and D. Li, "Electrophoretic motion of ideally polarizable particles in a microchannel," *Electrophor.*, vol. 30, no. 5, pp. 773–781, 2009.
[20] K. Khoshmanesh, S. Nahavandi, S. Baratchi, A. Mitchell, and K. Kalantar-Zadeh, "Dielectrophoretic platforms for bio-microfluidic systems," *Biosens. Bioelectron.*, vol. 26, no. 5, pp. 1800–1814, 2011.
[21] R. W. DeBlois, C. P. Bean, and R. K. A. Wesley, "Electrokinetic measurements with submicron particles and pores by the resistive pulse technique," *J. Colloid Interface Sci.*, vol. 61, no. 2, pp. 323–335, 1977.
[22] E. C. Gregg and K. D. Steidley, "Electrical counting and sizing of mammalian cells in suspension," *Biophys. J.*, vol. 5, no. 4, pp. 393–405, 1965.
[23] W. Xu, R. Mezencev, B. Kim, L. Wang, J. McDonald, and T. Sulcheck, "Cell stiffness is a biomarker of the metastatic potential of ovarian cancer cells," *PLOS ONE*, vol. 7, no. 10, p. e46609, 2012.
[24] S. Byun, S. Son, D. Amodei, N. Cermak, J. Shaw, J. H. Kang, V. C. Hecht, M. M. Winslow, T. Jacks, P. Mallick, and S. R. Manalis, "Characterizing deformability and surface friction of cancer cells," *Natl. Acad. Sci. USA*, vol. 110, no. 19, pp. 7580–7585, 2013.

Jinhong Guo received the B.E. degree in electronic engineering from the University of Electronic Science and Technology of China (UESTC), Sichuan, China, in 2010.

Currently, he is working toward the Ph.D. degree at Nanyang Technological University (NTU), jointly attached to the Institute of Microelectronics, A*STAR, Singapore. He has worked at the Applied Microfluidicology Lab at NTU, and as a Research Engineer in RFIC design at VIRTUS Integrated Circuit Design Lab at NTU until August 2011. His research interests include micro/nano solid-state biosensors, microfluidic electronics, optofluidic sensors, nano-electromagnetics, and microwave microfluidics.

Wen Lei received the B.E. degree in electronic engineering from the University of Electronic Science and Technology of China (UESTC), Sichuan, China, in 2012.

Currently, she is working toward the Ph.D. degree in the Department of Electrical and Computer Engineering, National University of Singapore (NUS), Singapore. Her research interests include implantable antenna design, bio-electromagnetics and microwave microfluidics, and biomedical sensors.

Xing Ma received the B.E. degree from the Harbin Institute of Technology, Heilongjiang, China.

Currently, he is working toward the Ph.D. degree at the School of Material Science and Engineering, Nanyang Technological University, Singapore. His research focus is on nano-materials for drug delivery.

Peng Xue received the M.Eng. degree in biomedical engineering from the Harbin Institute of Technology, Heilongjiang, China, in 2011.

Currently, he is a postgraduate student at Nanyang Technological University, Singapore. His research interests are droplet microfluidics, paper-based analytical devices, and electrochemical biosensing.

Yu Chen received the M.Sc. degree in physics from Fudan University, Shanghai, China, and the Ph.D. degree in physics from Boston University, Boston, MA, USA, in 2002 and 2008, respectively.

Currently, he is a Scientist at the Institute of Microelectronics, A*STAR, Singapore. His research interests include design and fabrication of nano-scale biosensors, and design and characterization of high throughput cell-based biosensor arrays.

Yuejun Kang received Ph.D. degrees in mechanical engineering from Nanyang Technological University (NTU), Singapore, and Vanderbilt University, Nashville, TN, USA, in 2005 and 2008, respectively.

His Ph.D. research focused on fundamental microfluidics, nonlinear electrokinetic phenomena, and development of integrated microdevices for biomedical detection and manipulation. Before he joined the School of Chemical Biomedical Engineering at NTU as an Assistant Professor in March 2011, he worked as a Postdoctoral Researcher at Monash University, Melbourne, Australia, and Los Alamos National Laboratory, Los Alamos, NM, USA. His current research is focused on micro/nano-fluidics based bio-instrumentation using electrical, optical, acoustical, and biochemical methods for analysis of biological cells/elements with biomedical, bio-energy, and environmental applications.